



# Physicomechanical properties of raw and comminuted pine and poplar shavings: energy consumption, particle size distribution and flow properties

Paweł Tryjarski<sup>1</sup> · Aleksander Lisowski<sup>1</sup> · Jakub Gawron<sup>2</sup> · Paweł Obstawski<sup>3</sup>

Received: 24 November 2022 / Accepted: 14 March 2023 / Published online: 25 March 2023  
© The Author(s) 2023

## Abstract

The aim of this study was to assess the energy consumption during milling and cutting-milling of pine and poplar shavings and the determination of particle size distribution (PSD) characteristics and mechanical properties of these materials. Cutting-milling process required less energy (in  $\text{kJ}\cdot\text{kg}^{-1}$ ) than milling but maximum mass flow rate of shavings was significantly higher and thus the effective power requirement of the knife mill during cutting also was higher. Comminution of plastic poplar shavings was more energy-consuming than harder pine shavings. These features influenced PSD, which was approximated with four mathematical models: Rosin–Rammler–Sperling–Bennett (RRSB), normal, logistic and lognormal. On the basis of the best fitting ( $R_{\text{adj}}^2$ ) for RRSB, detailed PSD parameters were calculated and all PSDs were described as ‘mesokurtic’, ‘fine skewed’ and ‘well-graded’. In comparison to milled shavings, cut-milled shavings had higher density, but were less compressible and had lower unconfined yield strength. However, cut-milled shavings had higher flowability because of lower cohesion and internal friction angles, because after cutting-milling particles were more spherical than elongated particles after milling. Cut-milled poplar shavings had more favourable mechanical parameters and better PSD characteristics, but required more energy for comminution than pine shavings.

---

✉ Aleksander Lisowski  
aleksander\_lisowski@sggw.edu.pl

<sup>1</sup> Department of Biosystems Engineering, Institute of Mechanical Engineering, Warsaw University of Life Sciences, Nowoursynowska 166, 02-787 Warsaw, Poland

<sup>2</sup> Department of Production Engineering, Institute of Mechanical Engineering, Warsaw University of Life Sciences, Nowoursynowska 166, 02-787 Warsaw, Poland

<sup>3</sup> Department of Fundamental of Engineering and Power Engineering, Institute of Mechanical Engineering, Warsaw University of Life Sciences, Nowoursynowska 166, 02-787 Warsaw, Poland

**List of symbols**

$A_{lg}, A_{ln}, A_n, A_R$	Coefficients for curves peaks in logistic, lognormal, normal and Rosin–Rammler–Sperling–Bennett model, respectively (mm)
$c$	Cohesion (kPa)
$C_g$	Coefficient of gradation
CI	Carr’s Compressibility Index
$C_u$	Coefficient of uniformity
$E_j$	Energy consumption during shavings comminution ( $\text{kJ}\cdot\text{kg}^{-1}$ )
$ff_c$	Flow index
HR	Hausner ratio
$I_u$	Uniformity index (%)
$K_g$	Graphic kurtosis
MC	Moisture content (% w.b.)
$m_d, m_i, m_m$	Mass of shavings comminuted in time $t$ , instantaneous and final, respectively (g)
$N$	Number of experimental data points in a sample
$n$	Rosin–Rammler–Sperling–Bennett’s particle size distribution parameter
$N_{sg}$	Size guide number, statistical particles size (mm)
$p$	Number of parameters in distribution density model
$P_b$	Idle power of knife mill (W)
$P_b, P_{b1}, P_{b2}$ and $P_{b3}$	Active power of three phases and active powers of subsequent phases, respectively (W)
$P_e, P_{ei}$	Effective and instantaneous power of knife mill, respectively (W)
$q_m$	Maximum mass flow rate ( $\text{g}\cdot\text{s}^{-1}$ )
$R^2$	Coefficient of determination (%)
$R_{\text{adj}}^2$	Adjusted coefficient of determination (%)
$s_g$	Standard deviation, dimensionless
$s_{gw}$	Standard deviation (mm)
$S_{ig}$	Inclusive graphic skewness
$S_l$	Mass relative span
$\text{STD}_h, \text{STD}_l$ , and $\text{STD}_t$	Geometric STD of high and low and total regions, respectively
$S_v$	Particle size variation ranges (%)
$t$	Comminution time (s)

$x_5, x_{10}, x_{16}, x_{25}, x_{30}, x_{50}, x_{60}, x_{75}, x_{84}, x_{90}$ and $x_{95}$	corresponding particle sizes at 5, 10, 16, 25, 30, 50, 60, 75, 84, 90 and 95 percentile of cumulative undersize mass distribution, respectively (mm)
$x_g$	Geometric mean of particle size (mm)
$x_{gm}$	Graphic mean of particle size (mm)
$x_R$	Particle size for 63.2% of mass distribution, Rosin-Rammler-Sperling-Bennett parameter (mm)
$\delta$	Angle of external friction for wood shavings-chrome steel ( $^\circ$ )
$\Delta t_{ke}, \Delta t_{km}$	Time interval in power and mass measurements, respectively (s)
$\lambda$	Knife mill loads equalizing lag time (s)
$\mu_{lg}, \mu_{ln}, \mu_n$	Particle size arithmetic means in logistic, lognormal and normal model, respectively (mm)
$\sigma$	Normal stress (kPa)
$\sigma_1$	Major consolidating stress (kPa)
$\sigma_c$	Unconfined yield strength (kPa)
$\sigma_{ig}$	Inclusive graphic standard deviation (mm)
$\sigma_{lg}, \sigma_{ln}, \sigma_n$	Particle size standard deviation in logistic, lognormal and normal model, respectively (mm)
$\tau$	Shear stress (kPa)
$\varphi$	Angle of internal friction ( $^\circ$ )
$\varphi_c$	Angle of internal friction for determined flowability ( $^\circ$ )
$\varphi_e$	Effective angle of internal friction ( $^\circ$ )
$\varphi_{lin}$	Linearized angle of internal friction ( $^\circ$ )
$\rho_a, \rho_t$	Aerated and tapped bulk density, respectively ( $\text{kg}\cdot\text{m}^{-3}$ )
PICM	Pine shavings, cut-milled
PIM	Pine shavings, milled
PIR	Pine shavings, raw
POCM	Poplar shavings, cut-milled
POM	Poplar shavings, milled
POR	Poplar shavings, raw

## Introduction

Wood shavings with particle size of 5–15 mm can be used directly to produce briquettes, but pellets production requires smaller particles, below 3.2 mm (Mani et al. 2003). In the mixture, smaller particles have higher specific surface, pore size and number of contact points, which is beneficial for interparticle bonding during agglomeration (Mani et al. 2004), increases bulk density and flowability of the biomass, decreases specific energy consumption during pelleting, and improves granulator performance and pellet quality (Mayer-Laigle et al. 2018).

Material fragmentation requires energy consumption, which depends on the biomass type, moisture, material properties, initial particle size, material feed rates (Miao et al. 2011) and type and working parameters of the machine: tip speed, milling yield, sieve size and clearance (Yu et al. 2003). The comminution processes may include one or a combination of the following operations: cutting, shearing, compressing, tearing (Miu et al. 2006) and coexisting fracture, breakage, impact crash and twisting (Oyedeki et al. 2020), friction and broken cohesion mechanisms (Jung et al. 2018).

Hammer mills, knife mills and linear knife grid mills (Pradhan et al. 2018), ball, beater, needle (pin) mills and shredders (Miao et al. 2011) were used for biomass grinding. Knife and hammer mills are most useful for wood grinding (Miu et al. 2006). Based on the literature, a hammer can be fixed or freely swinging (Yu et al. 2003), but more logical is the assumption that a hammer is fixed and a plate is freely swinging (Mugabi et al. 2019) and is termed as the beater. Knife mills, where cutting is a main process, are useful for grinding the plant material (Miu et al. 2006) and also work well at higher material moisture (Jewiarz et al. 2020). Hammer mills are able to grind harder materials with larger sizes (Miu et al. 2006) and are more suitable for materials with lower moisture (Jewiarz et al. 2020).

The use of a knife mill instead of a hammer mill allowed for a double reduction in grinding energy consumption (in  $\text{kJ}\cdot\text{kg}^{-1}$ ), with a slight deterioration of the grinding effect of Scots pine, European beech, cup plant and giant miscanthus (Jewiarz et al. 2020). Higher dust content in wood fuel powder was obtained by four different hammer mills than by a knife mill (Paulrud et al. 2002). Mixtures with higher dust content had stronger tendency to bridging, which was influenced by the shape and size of the particles.

Influence of moisture content, particle size and shape of hammer-milled poplar wood and corn stalks on the handling behaviour was analysed, and less bridging for mixtures with lower content of long and hook-shaped particles and better flow properties were found. Higher moisture is related to a greater angle of internal friction and a greater tendency to form arcs or ratholes (higher normal stresses) and more difficult rearrangement of particles, reducing the bulk density of the mixture (Gil et al. 2013).

Machines used in wood processing can perform various processes such as cutting, chipping, hammering and shredding and, depending on the purpose, various methods of measuring load and energy consumption are used (Warguła et al. 2022). Throughput and specific energy consumption of chippers or sawmills strongly depend on the raw materials, machine size, machine type, and specific machine settings, including knife (Kuptz and Hartmann 2014) and saw blade sharpness. Power metres for checking the quality of power, data loggers for a specific energy consumption trend (Gopalakrishnan et al. 2012) or electricity metres (Kuptz and Hartmann 2014) are used for energy analysis and diagnostics of electrical stationary woodworking equipment. The specific energy consumption needed for wood processing by machines powered by combustion engines can be determined on the basis of fuel consumption (Kuptz and Hartmann 2014) or by measuring the torque and rotational speed of the tractor PTO. Targeted research shows that individual machine settings, including regular knife sharpening or replacement, increase throughput and reduce energy consumption (Kuptz and Hartmann 2014).

There are related processes in the comprehensive technology of pressure agglomeration of biomass such as feeding, grinding, fluidisation, mechanical/pneumatic transport, blending, conditioning and storage in hoopers or bins (Xu et al. 2018). A stable and continuous flow of comminuted material is important in these processes, without the risk of its bridging, spontaneous agglomeration and separation. Understanding the comminuted biomass properties related to the flowability allows the design of reliable devices for its conversion. Stress caused by consolidation and design solutions of technical devices used for transport, conversion or storage affect the flow characteristics of the comminuted biomass (Stasiak et al. 2020).

Various test methods are used to assess the flowability of the comminuted biomass (powders). In the test for a non-compacted mixture, angle of repose, *AOR*, is determined (Stasiak et al. 2015). The particles packing properties in the mixture are determined in the tapping test, and Hausner ratio, *HR*, and Carr's Compressibility Index, *CI*, are calculated (Rezaei et al. 2016). A more precise test for quantitative measurement of the comminuted biomass flowability is the consolidated mixture test containing the standard shear procedure (Eurocode 1 2006), using the Jenike shear cell tester or the Shulze ring shear tester (Salehi et al. 2017). On the basis of shear results, materials can be quantified using unconfined yield strength,  $\sigma_c$ , flow index,  $ff_c$ , cohesion,  $c$  and angle of internal friction  $\varphi$  (Stasiak et al. 2020). It is assumed that materials with the cohesion less than 2 kPa and an angle of internal friction less than 30° can flow because of gravity (Fasina 2006). Tests on non-compacted or tapped materials are better suited for the classification of mixtures (powders), and the results of the shear tests can be helpful in the design of technical equipment, such as silos and feeders. The properties of loose materials allow to identify the cause of flow problems and differences between materials (Fasina 2006). The choice of the analytical technique for comminuted biomass assessment should be done on the basis of the ability to correctly restore the state of stresses and densification in a potential technological process (Jin et al. 2020). The result of the assessment of the comminuted material flowability is influenced by material properties: texture and surface roughness and moisture

content (Stasiak et al. 2020), particle size distribution and particles shape (Stasiak et al. 2019), the level of consolidation (Stasiak et al. 2018) and temperature of the system (Wilén and Rautalin 1995), (Tomasetta et al. 2014) and the ambient relative humidity (Ganesan et al. 2008).

However, there is a limited number of publications on the impact of the comminution method on the energy consumption of the process (Jiang et al. 2017), comminution energy efficiency (Eisenlauer and Teipel 2021), particle size distribution (Kratky and Jirout 2020) and flowability properties of wood shavings, intended for the production of internal layers of chipboards or briquettes, and after further shredding of the shavings for the production of pellets (Moiceanu et al. 2019).

The aim of this research was: (a) determination of energy consumption during milling or cutting-milling of pine and poplar shavings; (b) quantification of the effect of particle size on the wood shavings flowability properties; (c) development of parameters characterising physicommechanical properties for raw and comminuted wood shavings; (d) development of four mathematical models approximating PSD.

The novelty of this work is the comprehensive connection and analysis of PSD characteristics approximated by mathematical models with mechanical properties of pine and poplar shavings and with energy consumption during comminution of raw shavings intended for the production of particleboards or moulded solid fuel.

## Materials and methods

### Materials

The starting material for the research was pine and poplar wood. Pine wood was cut in a dedicated machine into shavings for production of particleboards, and poplar shavings were made of sawmill residues in a laboratory shredder. The raw shavings were obtained from the Research and Development Centre for Wood-Based Panels, Ltd. in Czarna Woda. Physicommechanical properties of wood shavings were investigated for three states: raw shavings, milled shavings and cut-milled shavings (Fig. S1 of SI). Milling and cutting-milling were conducted in the knife mill at Warsaw University of Life Sciences.

### Moisture content

The material moisture content was measured using the moisture analyser (MA50/1.R, Radwag, Radom, Poland) with an accuracy of 0.001% (weight measurement accuracy was 1 mg). Samples weighing approximately 2 g each were automatically analysed. Moisture was analysed fivefold and results variability was reported as a single standard deviation.

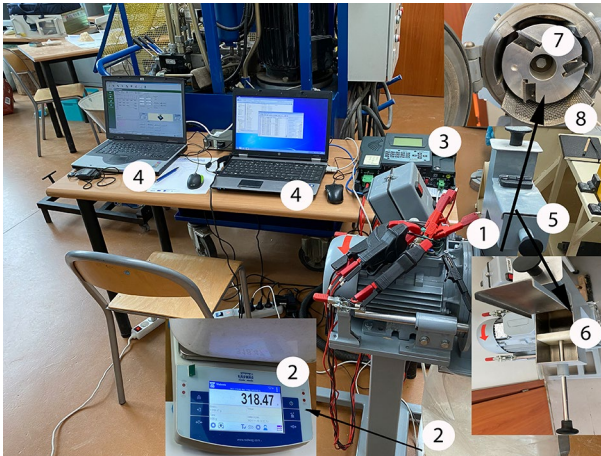


**Fig. 1** Stand for measuring the energy consumption during biomass comminution; 1–knife mill, 2–electronic scales, 3–power quality analyser, 4–laptops for data acquisition, 5–sample container, 6–feeding piston, 7–knife disc, 8–sieve with 3 mm mesh diameter

### Energy consumption measurements during raw shavings comminution

The stand for measuring the energy consumption of raw pine shaving comminution consisted of the knife mill (LMN-100, Alchem Group Ltd., Toruń, Poland), the power quality analyser EQUA Wally with WINEQUA software (Pro-Elektra, Olsztyn, Polska), the electronic scales WPS 600/C with PomiarWin software (Radwag, Radom, Poland) for mass recording via the RS 232 port and two laptops for data acquisition (Fig. 1).

The knife mill worked both, in counterclockwise and clockwise rotation. In counterclockwise rotation, the knives in cooperation with a 3 mm mesh sieve comminuted the material by grinding and tearing, without cutting. In clockwise rotation, the knives cut the shavings on the counter-cutting edge and subsequently ground, tore and cut them with 3 mm mesh sieve. These two shavings comminution modes were called milling and cutting-milling, respectively. The nominal rotational speed of rotor mill was 2880 rpm and peripheral cutting speed was  $15.39 \text{ m}\cdot\text{s}^{-1}$ . The clearance between cutting and counter-cutting edge was 1.15 mm and the knife blade angle was  $45^\circ$ . The knives were sharp. Comminuted shavings mass was weighed with an accuracy of 0.01 g and maximum possible frequency of 2 Hz, and the voltage and current on the three phases were measured with the maximum possible frequency of 50 Hz. A sample of raw shavings with a mass of 55 g was milled for about 35 s and cut-milled for about 10 s. Active power was measured in accordance with the PN-EN 50160 standard (PN-EN 50160 2014). The power quality analyser measured three states (Fig. 2); after turning on the power–power supply, after turning on the knife mill– idle power, during comminution–power required to drive the mill under load.

The active power on the engine was determined as a sum of the power from the three phases.

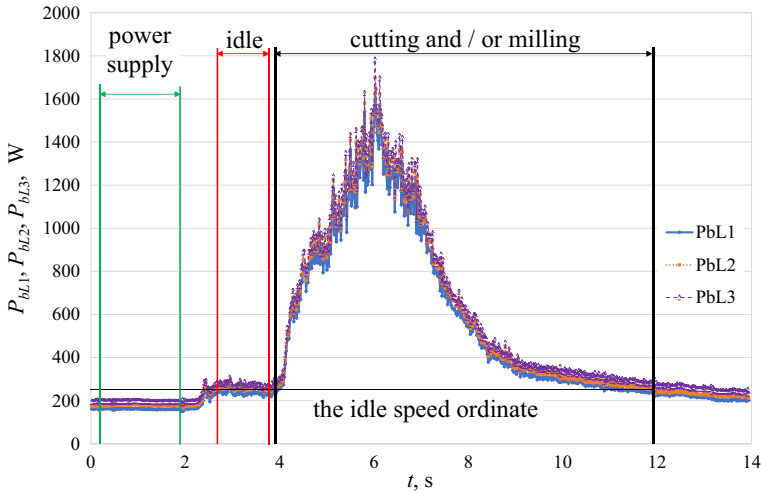


**Fig. 2** Example of knife mill power characteristics with marked areas: turning on the power supply, the idle power and the power of work under load;  $P_{bL1}$ ,  $P_{bL2}$ ,  $P_{bL3}$ —power on the three consecutive phases,  $t$ —time (points on the graph represent the instantaneous power values measured with 0.02 s interval)

$$P_b = P_{bL1} + P_{bL2} + P_{bL3} \tag{1}$$

where  $P_b$  is the active power of three phases, W;  $P_{b1}$ ,  $P_{b2}$  and  $P_{b3}$  are the active powers on the three consecutive phases, W.

The difference between the active power of knife mill under load  $P_b$  and the idling power  $P_i$  is the effective power, which is a work (energy) performed by the mill during comminution of shavings per unit of time.

$$P_e = P_b - P_i \tag{2}$$

where  $P_e$  is the effective power of the knife mill, W;  $P_b$  is the active power of the knife mill under load, W;  $P_i$  is the idling power of the knife mill, W.

Comminuted shavings mass was measured with an electronic scale as a cumulated value, therefore cumulated mass distribution  $m_c$  approximated by the modified Gompertz model (Velázquez-Martí et al. 2018), Eq. 3, was recalculated into the instantaneous mass distribution  $m_i$  (Fig. S2 of SI). After synchronisation against time, it can be superimposed on effective instantaneous power distribution  $P_{ei}$  (Fig. S3 of SI).

$$m_d = m_m \exp\left(-\exp\left(\frac{q_m e}{m_m}(\lambda - t) + 1\right)\right) \tag{3}$$

where  $m_d$  is the mass of comminuted shavings in time  $t$ , g;  $m_m$  is the final mass of comminuted shavings, g;  $q_m$  is the maximum mass flow rate, g·s<sup>-1</sup>;  $\lambda$  is the knife mill load equalizing lag time, s;  $t$  is the comminution time, s;  $e$  is the Euler number,  $e = 2.71$ .



An area under instantaneous power distribution is the work that needs to be done to mill shavings in the knife mill and the work-to-mass ratio is the energy consumption of the process, in  $\text{kJ}\cdot\text{kg}^{-1}$ . Energy consumption of comminution is the mean amount of energy used in the process of wood shavings comminution (milling or cutting-milling) per unit of dry matter. The areas under the curves of the instantaneous effective power and mass distribution were calculated by numerical integration using trapezoidal method and the energy consumption of wood shavings comminution,  $E_j$  (Eq. 4) was determined.

$$E_j = 10^{-3} \frac{\int P_{ei} dt}{\int m_i dt} = 10^{-3} \left( \sum_{k=1}^N \frac{P_{ei(t_{k-1})} + P_{ei(t_k)}}{2} \Delta t_{ke} \right) t / \left( \sum_{k=1}^N \frac{m_{i(t_{k-1})} + m_{i(t_k)}}{2} \Delta t_{km} \right) \quad (4)$$

where  $E_j$  is the energy consumption of shavings comminution,  $\text{kJ}\cdot\text{kg}^{-1}$ ;  $P_{ei}$  is the instantaneous effective power of the knife mill, W,  $m_i$  is the instantaneous shavings mass, kg;  $t$  is the comminution time, s;  $\Delta t_{ke}$  is the time interval in power measurements, s;  $\Delta t_{ke} = 0.02$  s;  $\Delta t_{km}$  is the time interval in mass measurements, s;  $\Delta t_{km} = 0.5$  s;  $k = 1, 2, 3, \dots, N$ ;  $N$  is the number of measurements for the analysed distribution.

Shavings moisture was measured before and after each series of 8–9 measurements for a given comminution system (wood species, comminution method). A moisture analyser (MA 50/1.R, Radwag, Radom, Poland) with a mass measurement accuracy of 0.1 mg was used to control the material moisture content.

### Particle size distribution

Raw shavings mixture samples with a volume of 10 l each were separated using the oscillating screen separator (Fig. S4 of SI), according to ANSI/ASAE S424.1 standard (ANSI/ASABE S424.1 2008). The sieve mesh sizes of 1.65, 5.61, 8.98, 18.0, 26.9 mm and a pan at the bottom in the set were used. The sample separation time was 120 s. The shavings after milling or cutting-milling were separated on a vibrating screen separator (LAB-11–200/UP, Eko-Lab, Brzesko, Poland) according to ANSI/ASAE S319.4 standard (ANSI/ASAE S319.4 2008). A double set of six sieves with dimensions of: 0.056, 0.1, 0.15, 0.212, 0.3, 0.425, 0.6, 0.85, 1.18, 1.6, 2.36, 3.35 mm and a pan at the bottom of each sieve set were used. 55 g samples were sieved for 600 s. The mass of the sample and separated fractions were weighed on an electronic scale (WPS 600/C, Radwag, Radom, Poland) with an accuracy of 0.01 g. Each separation was conducted in fivefold. Mass distribution in fractions and the mesh size allowed to calculate geometric mean of particle size ( $x_g$ ), standard deviation ( $s_g$ , dimensionless) and characteristic parameters of particle size distribution. Particle size distribution density was approximated by four models: Weibull (Weibull 1951), Rosin–Rammler–Sperling–Bennett (RRSB) (Rosin and Rammler 1933), Eq. 5, normal, Eq. 6, lognormal, Eq. 7 (Yang et al. 2012) and logistic, Eq. 8 (Weipeng et al. 2015), with modification of Su and Yu (2019).

$$f(x; x_R, n) = 100A_R \frac{n}{x_R} \left(\frac{x}{x_R}\right)^{n-1} \exp\left(-\left(\frac{x}{x_R}\right)^n\right) \quad (5)$$

$$f(x; \mu, \sigma) = \frac{100A_n}{\sigma_n \sqrt{2\pi}} \exp\left(-\frac{(x - \mu_n)^2}{2\sigma_n^2}\right) \quad (6)$$

$$f(x; \mu, \sigma) = \frac{100A_{ln}}{x \ln(\sigma_{ln}) \sqrt{2\pi}} \exp\left(\frac{-(\ln(x) - \ln(\mu_{ln}))^2}{2(\ln(\sigma_{ln}))^2}\right) \quad (7)$$

$$f(x; \mu, \sigma) = \frac{100A_{lg} \exp\left(\frac{-(x - \mu_{lg})}{\sigma}\right)}{\sigma_{lg} \left(1 + \exp\left(\frac{-(x - \mu_{lg})}{\sigma_{lg}}\right)\right)^2} \quad (8)$$

where  $f(x; x_R, n)$  and  $f(x; \mu, \sigma)$  are the density functions of the probability distribution, %;  $x$  is the particle size, mm;  $A_R$ ,  $A_n$ ,  $A_{ln}$  and  $A_{lg}$  are the coefficients for curve peaks in respective distributions, mm;  $x_R$  is the particle size for 63.2% of mass distribution, mm;  $n$  is the RRSB particle size distribution parameter (dimensionless);  $\mu$  is the particle size arithmetic mean (index indicates distribution model), mm;  $\sigma$  is the standard deviation (index indicates distribution model), mm; indexes  $n$ ,  $ln$  and  $lg$  are the indexes of normal, lognormal and logistic distribution models, respectively.

Selected models are widely used to describe particle size distributions of comminuted materials (Su and Yu 2019), whose cumulative distributions have a sigmoidal shape (Piątek et al. 2016). On the basis of the best-fitted RRSB density distribution model, the particle size distribution parameters were calculated. Calculation formulas are shown in supplementary material (Table S1 of SI).

## Packing properties test

In order to calculate parameters characterising packing indexes of wood shavings, aerated bulk density and tapped bulk density were calculated. Raw shavings density was tested in the cylinder with 154 mm diameter and 250 mm height, and the comminuted shavings' density was tested in the cylinder with size 53 mm and 160 mm, respectively, taking into account the requirement of tenfold cylinder size in comparison to average particle size. After putting shavings into cylinders, excess material was cutoff with a sharp steel plate with caution to not densify loose particles. Cylinder with shavings was weighted on an electronic scale (WPS 600/C, Radwag, Radom, Poland) with an accuracy of 0.01 g, and aerated bulk density  $\rho_a$  was calculated. Then, the cylinder with the shavings was mounted on the vibrating separator LAB-11-200/IP with a tapping frequency of 25 Hz and 2 mm vibration amplitude for 30 s tapping, with 750 stocks. Tapping parameters were based on the preliminary results, as after this time no density changes in the cylinder were observed. This criterion was used by Xu et al. (2018).

After tapping, the distance between the upper edge of the cylinder and the surface of material was measured using an electronic calliper with an accuracy of 0.01 mm. The measurements were taken on nine points: four at regular distance on each of two perpendicular diameters and one on the axis of the cylinder, similar to research conducted by Chevanan et al. (2010). The diameters of the circles were 82% and 58% of the cylinder diameter, dividing the surface into equal parts. The free volume above the shavings surface was subtracted from the total volume of the cylinder and with known shavings mass the tapped bulk density  $\rho_t$  was calculated. Measurement was taken fivefold. Based on these results, two important flowability parameters of wood shavings were calculated. One of them is a Hausner ratio (HR), which is the ratio of tapped bulk density to aerated bulk density, calculated according to Eq. 9 (Xu et al. 2018).

$$HR = \frac{\rho_t}{\rho_a} \quad (9)$$

where HR is the Hausner ratio (dimensionless);  $\rho_t$  is the tapped bulk density,  $\text{kg}\cdot\text{m}^{-3}$ ;  $\rho_a$  is the aerated bulk density,  $\text{kg}\cdot\text{m}^{-3}$ .

The second parameter is a Carr's Compressibility Index (CI), which is the ratio of difference between tapped bulk density and aerated bulk density to tapped bulk density, Eq. 10.

$$CI = \frac{\rho_t - \rho_a}{\rho_t} \quad (10)$$

### Strength and flowability

The materials strength and flowability were determined using a direct shear tester with a cylindrical cell with 60 mm internal diameter and 170 mm height. The tester was designed and manufactured according to Eurocode 1 standard (Eurocode 1 2006). The concept of this tester was based on Jenike apparatus and was improved using more modern technological solutions. The tester was powered by an AG 5089 hydraulic device (Fig. 3). Both devices were made by Rockfin Ltd., Nowy Tuchon, Poland. Tests were conducted for normal pressures of 20, 30, 40, 50 and 60 kPa, taking into account the mass of piston and analysed material bed above the shear plane, similar to Stasiak et al. (2015). Bed height after consolidation in each of the upper and lower cell parts was  $11.0 \pm 0.2$  mm. The lower cell part was being pushed with servomotor with  $0.048 \text{ mm}\cdot\text{s}^{-1}$  speed, and shear force was measured using a CL 17 strain gauge transducer with a measuring range up to 100 kN. The horizontal displacement of the lower cell part was measured with a laser distance gauge (LDS 100–500-S, Beta Sensorik). Fivefold tests were conducted for each combination of parameters. The data acquisition and control system consisted of a personal computer that controlled input/output (I/O) modules through a Hottinger Baldwin DMCplus (HBM, Darmstadt, Germany) high-speed digital interface card. The measurement and control systems were driven by CATMAN 2.1 software (HBM, Darmstadt, Germany), ensuring simultaneous acquisition of data and motion control at a sampling rate of 50 Hz.

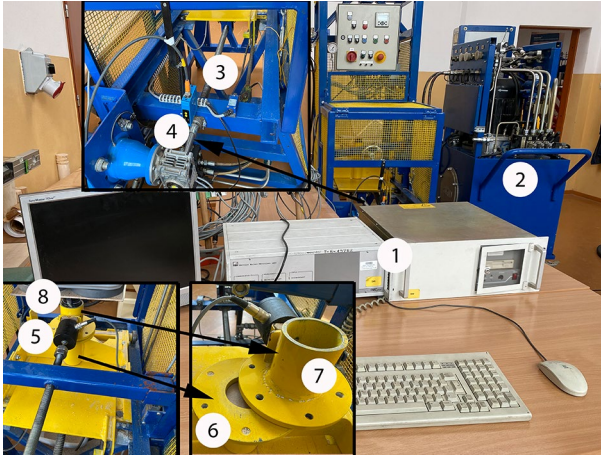


**Fig. 3** Test stand for direct shearing of comminuted material: 1–data acquisition system, 2–hydraulic attachment to drive the screw mechanism moving the lower part of the shearing cell, 3–screw mechanism driven by a hydraulic motor with a reductor, 4–laser distance gauge for lower part of shearing cell displacement measurements, 5–strain gauge for measuring shear force, 6–movable, lower shear cell with spacer discs to adjust the height of the material layer, 7–fixed, upper shear cell with a strain gauge, 8–piston with weights for material consolidation in the cell

With assumed normal stress values and experimental shear force–displacement curves, tangential stress  $\tau$ , Eq. 11, unconfined yield strength  $\sigma_c$ , Eq. 12, major consolidating stress  $\sigma_1$ , Eq. 13 and flow index  $ff_c$ , Eq. 14, were calculated (Littlefield et al. 2011).

$$\tau = \tan(\varphi)\sigma + c \quad (11)$$

$$\sigma_c = \frac{2c(1 + \sin\varphi)}{\cos\varphi} \quad (12)$$

$$\sigma_1 = \left( \frac{A - \sqrt{A^2 \sin^2 - \tau_{ssp}^2 \cos^2 \varphi}}{\cos^2 \varphi} \right) (1 + \sin\varphi) - \frac{c}{\tan\varphi} \quad (13)$$

$$ff_c = \frac{\sigma_1}{\sigma_c} \quad (14)$$

where  $A = \sigma_{ssp} + c/\tan\varphi$ ,  $\tau$  is the shear stress, kPa;  $\sigma$  is the normal stress, kPa;  $\varphi$  is the angle of internal friction, °;  $c$  is the cohesion, kPa;  $\sigma_c$  is the unconfined yield strength, kPa;  $\sigma_1$  is the major consolidating stress, kPa;  $ff_c$  is the flow index and subscript ssp designates the value at the steady state point.

Moreover, based on the experimental curves, the angle of internal friction was calculated (Stasiak et al. 2019). To characterise the material flow, Jenike (1961) proposed to use a major consolidating stress  $\sigma_1$  to unconfined yield strength  $\sigma_c$  ratio, called the flow index  $ff_c$ , a reciprocal of flow function FF. The flow index allows to classify materials as non-flowing:  $ff_c \leq 1$ , very cohesive:  $1 < ff_c < 2$ , cohesive:  $2 < ff_c < 4$ , easy flowing:  $4 < ff_c < 10$  and free flowing:  $ff_c \geq 10$ .

### Angle of external friction shavings-chrome steel

The angle of external friction  $\delta$  for various forms of wood shavings on the chrome steel plate surface, a material of which the agglomeration die was made, was determined by measuring the angle with an electronic protractor. The angle was determined as the minimal slope when particles of material started moving as the plate slope increased. A material sample was evenly distributed over the plate surface, while maintaining a layer thickness close to that of single particles. Measurements were taken five times for each system.

### Parameters selection

Parameters assessing physicochemical properties of wood shavings were selected by a feature correlation method to eliminate parameters whose values were strongly correlated. The selection aimed to reduce the parameter number to the proposed  $7 \pm 2$  (Miller 1994), increasing information processing perception by humans.

The input to analysis was the correlation coefficient matrix  $\mathbf{R}$  determined for the analysed parameters, for which the inverse matrix  $\mathbf{R}^{-1}$  was created,  $\mathbf{R}^{-1} = \mathbf{R}^T / \det(\mathbf{R})$ , where  $\mathbf{R}^T$  is the transposed matrix  $\mathbf{R}$ ,  $\det(\mathbf{R})$  is a determinant of the matrix  $\mathbf{R}$  (condition  $\det(\mathbf{R}) \neq 0$  must be satisfied). For parameter strongly correlated with others, elements of  $\mathbf{R}^{-1}$  exceeded the value of 10. That meant wrong numerical determination of the  $\mathbf{R}$  matrix. The parameter was removed from the starting parameters set if the diagonal value was  $\geq 10$ . Parameters were cyclically eliminated after one parameter strongly correlated with others had been removed, the procedure was repeated. The correctness of the obtained results was checked by calculating the identity matrix  $\mathbf{I}$ ,  $\mathbf{I} = \mathbf{R} \cdot \mathbf{R}^{-1}$ .

Correlation coefficient matrices were calculated in Statistica v.13.3 software (StatSoft Poland Ltd., Cracow). The determinant of matrix  $\mathbf{R}$  ( $\det(\mathbf{R})$ ), inverse matrices  $\mathbf{R}^{-1}$  and identity matrix  $\mathbf{I}$  were calculated in Excel.

### Statistical analysis

For the calculated parameters, characterising physicochemical properties of shavings, normality distributions were analysed using Kolmogorov–Smirnov (K–S) and Lilliefors correction (K–S–L) and Shapiro–Wilk (S–W) tests. Homogeneity of variance for these parameters for different factors (wood species and shavings forms) was tested with Levene and Brown–Forsythe tests. According to K–S test results,

$H_0$  hypothesis assuming normal distribution of these parameters (the  $p$  value was greater than 0.20 for all cases) cannot be rejected. Based on the results of the Levene and Brown–Forsythe tests, it can be concluded that for most of the analysed parameters there is no reason to reject the  $H_0$  hypothesis of homogeneity of variance between the analysed factors.

The data were analysed for the influence of factors (wood species, form of shavings (raw, milled, cut-milled)) on the physico-mechanical properties of mixtures (energy consumption parameters, particle size distribution parameters, flowability and direct shear strength) with multivariate analysis of variance MANOVA with Fisher–Snedecor ( $F$ ) test. Statistical significance of differences between mean values of parameters was checked by the Tukey’s test. Pearson correlation coefficient value matrices were analysed and evaluated by synonyms for the descriptors (Hopkins 2000). The analysis was conducted at the significance level  $p=0.05$ . Cohesion and angle of internal friction were determined with linear regression and parameters of nonlinear models with nonlinear estimation procedure. Goodness of fit for models to experimental data was evaluated with adjusted coefficient of determination,  $R_{\text{adj}}^2$  (Su and Yu 2019), which is a better criterion than coefficient of determination, Eq. 15.

$$R_{\text{adj}}^2 = 1 - \frac{(1 - R^2)(N - 1)}{(N - p - 1)} \quad (15)$$

where  $R_{\text{adj}}^2$  is the adjusted coefficient of determination (expressed in %);  $R^2$  is the determination coefficient (dimensionless);  $N$  is the number of experimental data points in a sample;  $p$  is the number of parameters in distribution density model.

Statistical analysis of research results was done in Statistica v.13.3 software (Stat-Soft Poland Ltd., Cracow, Poland).

## Results and discussion

### Comminution energy consumption of pine and poplar shavings

The starting physical parameters of raw pine and poplar shavings were similar as their moistures were 7% (Table 1) and geometric means of particle size  $x_g$  were 6.21 mm and 5.94 mm, respectively (Table S2 of SI). Comminution times of raw shavings samples weighing 47–50 g were almost 4-times longer during milling than cutting-milling and were 26.5–28.0 s and 6.9–7.9 s, respectively (Table 1).

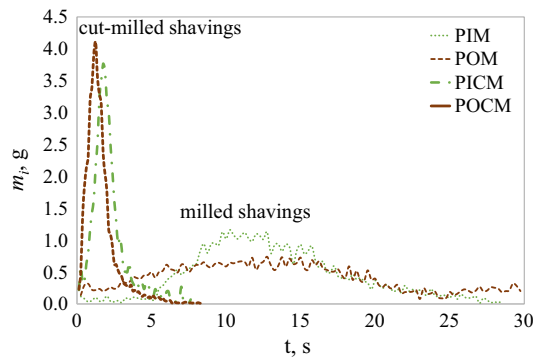
Extending the milling process in comparison to cutting-milling substantially reduced the load of the knife mill in the time domain (Fig. 4), and the effective power requirement of the mill was almost 3-times lower during milling than cutting-milling and amounted to 428–675 W and 1352–1660 W, respectively (Table 1). With such reversed relations of effective power against comminution time, the energy consumption of milling was 29% and 40% higher than those of cutting-milling for pine and poplar shavings, respectively. The energy consumption for milling the pine and poplar shavings was 234 and 417  $\text{kJ}\cdot\text{kg}^{-1}$  (189 and 521  $\text{kWh}\cdot\text{t}^{-1}$ ), respectively, and for cutting-milling 182 and 293  $\text{kJ}\cdot\text{kg}^{-1}$  (23 and 33  $\text{kWh}\cdot\text{t}^{-1}$ ), respectively. In

**Table 1** Average values and standard deviations of shavings moisture content, milling and cutting-milling parameters of pine and poplar shavings and modified Gompertz model parameters and their fit assessment

Parameter	Milled shavings		Cut-milled shavings	
	Pine	Poplar	Pine	Poplar
Moisture content, MC, %	6.90 <sup>a*</sup> ± 0.12	7.02 <sup>a</sup> ± 0.04	6.90 <sup>a</sup> ± 0.12	7.02 <sup>a</sup> ± 0.04
Sample mass, $m_d$ , g	48.3 <sup>a</sup> ± 1.2	47.0 <sup>a</sup> ± 2.8	50.1 <sup>a</sup> ± 0.9	48.4 <sup>a</sup> ± 2.1
Comminution time, $t_w$ , s	26.5 <sup>b</sup> ± 1.1	28.0 <sup>c</sup> ± 1.1	6.9 <sup>a</sup> ± 0.6	7.9 <sup>a</sup> ± 0.3
Effective power, $P_e$ , W	428 <sup>a</sup> ± 25	675 <sup>b</sup> ± 36	1352 <sup>c</sup> ± 99	1660 <sup>d</sup> ± 160
Energy consumption, $E_j$ , kJ·kg <sup>-1</sup>	234 <sup>b</sup> ± 14	417 <sup>d</sup> ± 35	182 <sup>a</sup> ± 18	293 <sup>c</sup> ± 25
Maximum mass, $m_m$ , g	49.3 ± 1.8	50.6 ± 3.7	48.8 ± 0.7	47.6 ± 2.3
Mass flow rate, $q_m$ , g·s <sup>-1</sup>	4.45 ± 0.47	2.88 ± 0.17	28.77 ± 2.39	31.99 ± 1.64
Lag feed, $\lambda$ , s	6.89 ± 0.86	3.85 ± 1.86	0.95 ± 0.27	0.53 ± 0.27
Coefficient of determination, $R^2$ , %	99.90 ± 0.06	99.84 ± 0.07	99.53 ± 0.16	99.39 ± 0.58
Global error, $d_g$ , %	1.83 ± 0.65	2.06 ± 0.58	3.35 ± 0.91	2.22 ± 0.62

\*In each row, differences between values with the same letter are statistically insignificant at  $p < 0.05$

**Fig. 4** Mass distribution of milled and cut-milled pine and poplar shavings during the comminution of raw material; PIM–milled pine shavings, POM–milled poplar shavings, PICM–cut-milled pine shavings, POM–cut-milled poplar shavings



comparative pine wood comminution studies, the energy consumption of the hammer mill is twice as high as that of the knife mill (Jewiarz et al. 2020) although absolute values are significantly lowered and probably false.

Under optimal working conditions of hammer mills, the energy consumption of milling pine wood to particle size of  $d_{50} = 0.5$  mm was 170 kWh·t<sup>-1</sup> and for poplar 130 kWh·t<sup>-1</sup> (Esteban and Carrasco 2006), therefore it was a reverse relation to the present results. This was due to almost twice the moisture contents of these materials (14.25% and 11.89%, respectively) and the inverse relationship of moisture to our shavings. As mentioned, the energy consumption of milling depends on many factors, including the degree of particle size reduction. Hammer grinding of pine particles from 3.59 mm to 2.19 mm consumed 15.9 kJ·kg<sup>-1</sup> energy (Naimi et al. 2016). Other studies indicate that the energy consumption of milling loblolly pine shavings with 4.7% moisture on 1.20 mm and 3.18 mm sieve size was 125 and 82 kJ·kg<sup>-1</sup>,



respectively (Hehar 2013). For comparison, a typical milling energy consumption of hard coal is  $7\text{--}36 \text{ kWh}\cdot\text{t}^{-1}$ .

Cutting-milling was more energy efficient, when sharp cutting edges of the knife were cutting shavings and subsequently cut-off particles were mashed through a sieve, than milling, when shavings were probably crushed, torn, bent, sheared and twisted by the beats of the knife plates and later mashed through a sieve (Miu et al. 2006). These complex processes were probably dependent on instantaneous position of the particles in relation to the knife, as well as the sieve and the counter-cutting edge, which also participated in comminution. The longer milling time allows the conclusion that the raw shavings were repeatedly rotated before fragmentation into particles with sizes that allowed them to pass through the sieve of the knife mill. Comminution of poplar shavings was more energy-consuming than pine shavings and was 78% and 61% greater during milling and cutting-milling, respectively. In comparison to pine shavings, longer milling time of poplar shavings and higher energy consumption during comminution were caused by lower strength parameters of poplar wood than pine wood. Energy consumption and particle size can be different for the same material with different moisture content, because the strength properties of wood depend on the moisture content, and what is important not always linearly dependent (Gerhards 1982). Poplar wood vs. pine wood at 16.1% and 13.5% moisture, respectively, has a hardness of 27 MPa and 29 MPa, compression strength perpendicular to grain of 1.9 MPa and 2.2 MPa, compression strength parallel to the grain of 18.2 MPa and 26.9 MPa, bending strength in the direction perpendicular to the grain of 40.2 MPa and 56.8 MPa, bending strength in the direction parallel to the grain of 2.2 MPa and 2.8 MPa, and modulus of elasticity of 5 860 MPa and 12 750 MPa, respectively (Aydin et al. 2007). This variability in the strength properties of wood significantly affected the variability in energy consumption in the comminution process. Under the pressure of the milling elements, the more plastic poplar vs. pine wood was crushed and macerated to a greater extent, without splitting it into smaller particles. The harder pine cracked and crumbled more than poplar wood. These crushed and squeezed particles required more force cycles than the milling elements in order to achieve the size that allowed the particles to pass through the sieve. The consequence of the particles flattening was a longer size of the milled poplar vs. pine shavings. A bigger particle size of milled poplar vs. pine shavings was a result of particles squeezing. The explanation of this process has not been presented in the available literature so far.

Although, the pressure on the feed piston was the same, the maximum mass flow rate  $q_m$  was 6–11 times greater during cutting-milling than cutting. The maximum mass flow rate  $q_m$  was determined on the basis of the modified Gompertz model, which approximated the cumulative mass flow rate very well;  $R^2=99.39\text{--}99.90\%$  and a global error of fit was 1.83–3.35% (Table 1). The results of the analysis showed that a more powerful electric motor is required during cutting-milling than during milling. However, the energy consumption during cutting-milling is lower and more favourable and more plastic poplar shavings are more difficult to comminute than harder pine shavings.



## PSD of milled and cut-milled pine and poplar shavings

PSD of raw pine and poplar shavings was bimodal and unimodal, respectively (Fig. S5 of SI).

In the bimodal PSD of raw pine shavings, there was a large share (29.5%) of fine particles with a size of 3.04 mm and large particles of 12.71 mm (37.0% share). These shares exceeded the share (26.9%) for geometric mean of particle size value of 6.21 mm. The bimodal distribution could result from the wood cutting process involving the cutting of large shavings 30–100 mm length, 20–25 mm width, 4–6 mm thickness, a varied pine wood structure or a variable tearing mechanism of solid pine wood with clear heartwood is visible harder than sapwood. In raw poplar shavings the PSD share of particles around maximum value was more aligned, which resulted from the less differentiated hardwood and sapwood compared to pine wood. Since the bimodality was not very high, the PSD was analysed as stochastic homogenous distribution (Rasteiro et al. 2008).

The PSDs differed according to the species of wood and the method of comminution by milling and cutting-milling during energetic conversion of raw shavings. Milled pine shavings PSD had a lower geometric mean of particle size  $x_g$  (0.60 mm) than poplar shavings (0.62 mm) and similarly the dimensionless standard deviation,  $s_g$  (2.06 and 2, 10, respectively) and standard deviation  $s_{gw}$  (2.29 mm and 2.49 mm, respectively). Different PSDs were obtained after cutting-milling, as  $x_g$  for pine shavings was 0.51 mm, and for poplar shavings was 0.45 mm, respectively; however,  $s_g$  was 1.89 and 2.03, and  $s_{gw}$  was 1.63 mm and 1.70 mm, respectively. It was probably a result of the domination of cutting and tearing instead of cutting by knives, where clearance of knife to counter-cutting edge was 15 mm and harder pine wood was crumbling into relatively larger particles than plastic poplar wood.

Among the four models, the RRSB was the best fit to the PSD as adjusted coefficient of determination  $R_{adj}^2$  was the highest and amounted to 81.19–98.66%, average 94.37% (Table 2). In the matched ranking, the next places were taken by the following models: normal (on average  $R_{adj}^2 = 93.03\%$ ), logistic (90.70%) and lognormal (88.41%).

The characteristics of particle sizes determined in models were oversized in relation to the geometric mean of particle size  $x_g$ , which is determined at 50% of mass distribution. According to the theory by Rosin and Rammler (1933), the  $x_R$  parameter is determined particle size for 63.2% of cumulative mass distribution undersize, and,  $\mu_{lg}$ ,  $\mu_{ln}$ ,  $\mu_n$  are the particle size arithmetic means in logistic, lognormal and normal models, respectively, which by definition are greater values than the geometric mean. The PSD of raw shavings was relatively flatter than the PSD of milled and cut-milled shavings, because  $n$  values in RRSB model were 1.88–1.94, 3.00–2.55 and 2.53–2.75, respectively. Larger standard deviations of the particle size in models represent wider PSD and for raw and milled shavings, they were proportional to the standard geometric dimensional deviations  $s_{gw}$ . Comparing the PSD characteristics of shavings, it can be stated that cutting-milling caused more even PSD than milling. During the cutting-milling process, raw shavings were cut and smaller particles

**Table 2** Fitting of the coefficients of the RRSB, normal, lognormal and logistic models of PSD densities for pine and poplar shavings, raw, milled, cut-milled and goodness of fit evaluation with  $R_{adj}^2$

Model	Parameters	Raw shavings		Milled shavings		Cut-milled shavings	
		Pine	Poplar	Pine	Poplar	Pine	Poplar
RRSB	$A_R$ , mm	5.46	4.95	0.23	0.26	0.21	0.18
	$x_R$ , mm	12.39	10.24	0.98	1.12	0.86	0.76
	$n$	1.88	1.94	3.00	2.55	2.53	2.75
	$R_{adj}^2$ , %	81.19	93.56	97.79	98.66	96.65	98.39
Normal	$A_n$ , mm	5.60	4.91	0.23	0.25	0.21	0.18
	$\mu_n$ , mm	9.96	8.16	0.86	0.95	0.74	0.66
	$\sigma_n$ , mm	5.95	4.72	0.33	0.41	0.33	0.27
	$R_{adj}^2$ , %	82.03	85.01	98.35	98.57	95.26	98.94
Lognormal	$A_{ln}$ , mm	6.57	5.56	0.25	0.29	0.23	0.20
	$\mu_{ln}$ , mm	12.34	9.20	0.92	1.07	0.81	0.72
	$\sigma_{ln}$ , mm	2.43	2.11	1.54	1.73	1.78	1.64
	$R_{adj}^2$ , %	70.33	93.46	93.74	91.17	89.85	91.93
Logistic	$A_{lg}$ , mm	3.85	3.47	0.15	0.17	0.14	0.12
	$\mu_{lg}$ , mm	10.08	8.23	0.85	0.95	0.75	0.66
	$\sigma_{lg}$ , mm	4.94	4.17	0.25	0.33	0.27	0.22
	$R_{adj}^2$ , %	78.71	81.58	98.81	96.24	90.96	97.91

$A_{lg}$ ,  $A_{ln}$ ,  $A_n$ ,  $A_R$ , coefficients for curve peaks in logistic, lognormal, normal and RRSB, respectively;  $x_R$ , particle size for 63.2% of mass distribution, RRSB parameter;  $n$ , RRSB particle size distribution parameter;  $\sigma_{lg}$ ,  $\sigma_{ln}$ ,  $\sigma_n$ , particle size standard deviation in logistic, lognormal and normal model, respectively;  $\mu_{lg}$ ,  $\mu_{ln}$ ,  $\mu_n$ , particle size arithmetic mean in logistic, lognormal and normal model, respectively;  $R_{adj}^2$ , adjusted coefficient of determination

were impacted, abraded, and pressed against the sieve for further reduction in particle sizes.

Detailed distribution parameters were calculated on the basis of the best-fit RRSB to PSD model (Table S2 of SI). 24 parameters in a feature correlation procedure were removed because they had very high positive values of Pearson correlation coefficients,  $r=0.728-0.999$ . Five parameters were left after this elimination: geometric mean of particle size  $x_g$ , standard deviation, dimensionless  $s_g$ , uniformity index  $I_u$ , coefficient of gradation  $C_g$  and graphic kurtosis  $K_g$ . The first two parameters;  $x_g$  and  $s_g$  are described above. The best uniformity of the particle sizes was characteristic for cut-milled pine shavings,  $I_u=11.57\%$ , in contrast to the lowest value of  $I_u=8.00\%$  for poplar shavings. More uniform were poplar than pine shavings after milling with  $I_u$  of 9.75% and 8.61%, respectively. Raw shavings were more diversified in case of uniformity as the  $I_u$  was 9.41% and 6.65% for pine and poplar, respectively. A reversed correlation characterised the coefficient of gradation  $C_g$ , which was within the narrow range of 1.17–1.22 for all mixtures and it indicated that PSD was well-graded, as it was within the range of 1–3 (Budhu 2007). The inverse relations of  $I_u$  to  $C_g$  are logical as PSD

of good particle size uniformity had large proportions of particles with sizes adjacent to the mode value (Figs. S5b, d, e of SI). For milled and cut-milled shavings, the proportion of particles around the mode value ranged from 73–79%, and for raw shavings it was even higher and amounted to 93–97%. Particle size gradation sequence could not be expected with such aligned particles, around mode value. The more uniform PSD, the less leptokurtic the distribution with lower graphic kurtosis  $K_g$ . The PSD of cut-milled pine shavings was the least leptokurtic,  $K_g=0.97$ . Since the  $K_g$  values were in the very narrow range of 0.97–1.00, all PSDs can be classified as “mesokurtic” ( $0.90 \leq K_g \leq 1.11$ ) (Blott and Pye 2011). Moreover, the inclusive graphic skewness was 0.20–0.30, and the lowest was for cut-milled pine shavings PSD ( $S_{ig}=0.20$ ) and for all PSDs was within the range of 0.20–0.30, so all PSDs can be classified as „fine skewed” ( $+0.1 \leq S_{ig} \leq +0.3$ ).

### Packing properties and shear test

Raw shavings, with significantly larger particles than comminuted shavings, were characterised by a lower compressibility ( $HR=1.15$ – $1.17$  and  $HR=1.38$ – $1.57$ , respectively, and  $CI=0.14$  and  $CI=0.27$ – $0.36$ , respectively), lower flowability ( $ff_c=4.29$ – $4.45$  and  $ff_c=4.29$ – $15.22$ , respectively) and greater cohesion ( $c=8.5$ – $11.0$  and  $c=2.3$ – $8.7$ , respectively), and met the practical requirements:  $HR < 1.25$  and  $CI=0.05$ – $0.15$  (Table 3) (Stasiak et al. 2015).

Raw shaving can be classified between cohesive and easy flowing materials. In relation to the raw shavings, both packing indexes HR and CI increased with decreasing particle size of shavings, which was reflected in negative Pearson correlation coefficients,  $-0.8875$  and  $-0.9188$ , respectively (very high and almost full correlation, respectively). Cut-milled shavings with particles smaller than the particles of milled shavings had a higher tapped bulk density (by 14%) and aerated bulk density (by 24%), but the ratios of these densities, HR were opposite and amounted to 1.52 and 1.39, respectively. In comparison to the larger milled particles, the voids formed between smaller cut-milled particles were more easily filled by fine particles, whose share in the mixture was high.

Tapping caused easier dislocation, collapsing and consolidation in case of smaller cut-milled particles vs. larger ones, increasing the density. The finer cut-milled particles were more spherical than elongated particles left after milling and therefore, HR was lower, confirming Hausner’s observations (Beaunac et al. 2022). Cut-milled poplar shavings had higher packing and flowability than cut-milled pine shavings, because poplar shavings were smaller and, as mentioned, were more plastic than pine shavings. Larger differences in the flowability properties were found for cut-milled shavings than for milled ones, as the cohesions were 2.3 and 3.9 and 8.3 and 8.7, respectively and it was caused by differences in particle sizes. As  $x_g$  dimensions decreased, the  $ff_c$  increased (negative correlation,  $r=-0.410$ ) and  $c$  decreased (positive correlation,  $r=0.438$ ), which indicates that cohesion of finer cut-milled shavings decreased and their flow became better. Similar results were found by Xu et al. (2018) in case of coal and glass powders. The  $ff_c$  and  $c$  were strongly influenced by preconsolidation stress,  $\sigma$ , which caused

**Table 3** Average values and standard deviations of mechanical parameters of raw, milled and cut-milled pine and poplar shavings

Parameter	Raw shavings		Milled shavings		Cut-milled shavings	
	Pine	Poplar	Pine	Poplar	Pine	Poplar
$\rho_a$ , kg·m <sup>-3</sup>	116 <sup>a*</sup> ± 4	120 <sup>a</sup> ± 1	200 <sup>c</sup> ± 2	155 <sup>b</sup> ± 4	229 <sup>d</sup> ± 1	213 <sup>c</sup> ± 1
$\rho_r$ , kg·m <sup>-3</sup>	135 <sup>a</sup> ± 4	139 <sup>a</sup> ± 2	294 <sup>c</sup> ± 5	243 <sup>b</sup> ± 5	315 <sup>d</sup> ± 4	297 <sup>c</sup> ± 5
HR	1.17 <sup>a</sup> ± 0.04	1.15 <sup>a</sup> ± 0.01	1.47 <sup>c</sup> ± 0.04	1.57 <sup>d</sup> ± 0.03	1.38 <sup>b</sup> ± 0.01	1.39 <sup>b</sup> ± 0.02
CI	0.14 <sup>a</sup> ± 0.03	0.14 <sup>a</sup> ± 0.01	0.32 <sup>c</sup> ± 0.02	0.36 <sup>d</sup> ± 0.01	0.27 <sup>b</sup> ± 0.01	0.28 <sup>b</sup> ± 0.01
$\tau$ , kPa	38.0 <sup>d</sup> ± 2.6	27.7 <sup>b</sup> ± 0.7	35.4 <sup>d</sup> ± 3.2	31.8 <sup>c</sup> ± 0.8	26.8 <sup>b</sup> ± 0.3	19.8 <sup>a</sup> ± 0.2
$c$ , kPa	11.0 <sup>c</sup> ± 5.7	8.5 <sup>ab</sup> ± 2.4	8.7 <sup>ab</sup> ± 5.5	8.3 <sup>ab</sup> ± 1.8	3.9 <sup>a</sup> ± 1.7	2.3 <sup>a</sup> ± 0.7
$R^2$ , %	98.61	99.02	98.71	99.85	99.83	99.99
$\sigma_1$ , kPa	140 <sup>c</sup> ± 19	109 <sup>ab</sup> ± 6	134 <sup>bc</sup> ± 27	119 <sup>abc</sup> ± 13	120 <sup>abc</sup> ± 5	98 <sup>a</sup> ± 2
$\sigma_c$ , kPa	40.0 <sup>d</sup> ± 18.1	26.8 <sup>abc</sup> ± 6.1	30.1 <sup>bc</sup> ± 14.9	28.8 <sup>bc</sup> ± 4.9	13.4 <sup>ab</sup> ± 5.5	7.1 <sup>a</sup> ± 2.0
$ff_c$	4.45 <sup>a</sup> ± 2.95	4.29 <sup>a</sup> ± 1.14	6.15 <sup>a</sup> ± 4.40	4.29 <sup>a</sup> ± 1.15	10.92 <sup>ab</sup> ± 6.42	15.22 <sup>b</sup> ± 6.11
$\varphi_e$ , °	40.0 <sup>d</sup> ± 1.7	31.5 <sup>b</sup> ± 0.9	37.9 <sup>cd</sup> ± 4.7	35.0 <sup>bc</sup> ± 1.7	32.4 ± 0.6	25.3 <sup>a</sup> ± 0.2
$\varphi_c$ , °	23.9 <sup>c</sup> ± 2.6	17.8 <sup>ab</sup> ± 1.6	23.0 <sup>bc</sup> ± 6.1	21.0 <sup>abc</sup> ± 1.6	21.0 <sup>abc</sup> ± 1.2	16.2 <sup>a</sup> ± 0.5
$\varphi_{lin}$ , °	33.8 <sup>c</sup> ± 4.2	25.6 <sup>ab</sup> ± 2.7	33.1 <sup>bc</sup> ± 8.4	30.4 <sup>abc</sup> ± 2.2	29.7 <sup>abc</sup> ± 1.7	23.7 <sup>a</sup> ± 0.6
$\delta$ , °	15.1 <sup>a</sup> ± 0.7	19.1 <sup>b</sup> ± 0.8	29.7 <sup>c</sup> ± 1.0	28.1 <sup>c</sup> ± 0.5	34.7 <sup>c</sup> ± 0.7	32.2 <sup>d</sup> ± 1.4

\*In each row, differences between values with the same letter are statistically insignificant at  $p < 0.05$

$\rho_a$ , aerated bulk density;  $\rho_r$ , tapped bulk density; HR, Hausner ratio; CI, Carr’s Compressibility Index;  $\tau$ , shear stress;  $c$ , cohesion;  $R^2$ , coefficient of determination;  $\sigma_1$ , major consolidating stress;  $\sigma_c$ , unconfined yield strength;  $ff_c$ , flow index;  $\varphi_e$ , effective angle of internal friction;  $\varphi_c$ , angle of internal friction for determined flowability;  $\varphi_{lin}$ , linearized angle of internal friction;  $\delta$ , angle of external friction wood shavings-chrome steel

shavings rearrangement creating tight, packed beds, which resulted in an increase in shear stress  $\tau$  (Fig. S6 of SI). The highest  $\tau$  vs.  $\sigma$  characterised the raw pine shavings and higher  $\tau$  values and bigger dynamic of changes were in the case of pine shavings rather than poplar ones (Fig. 5), and the evidence for that is  $\varphi_{lin}$  values (Table 3). Together with the decrease in particle size of comminuted shavings,  $\tau$  decreased (positive correlation,  $r=0.363$ ). The highest consolidating stress  $\sigma_1$  and unconfined yield strength  $\sigma_c$  were greater in case of pine shavings than poplar shavings and decreased with  $x_g$ ; however, positive correlation  $r=0.461$  was noticed only between  $\sigma_c$  and  $x_g$ . The finer the shavings, the lower the unconfined yield strength.

The angles of internal friction  $\varphi_e$ ,  $\varphi_c$  and  $\varphi_{lin}$  were greater in case of pine shavings than poplar shavings and were characterised by high correlation coefficients values between them,  $r=0.873-0.983$ . These friction angles tended to decrease with particle size decrease (Table 3), but no correlation was noticed between these parameters. The angles of internal friction  $\varphi_e$ ,  $\varphi_c$  and  $\varphi_{lin}$  very highly correlated with  $\tau$  ( $r=0.720-0.958$ ) and with  $\sigma_1$  ( $r=0.881-0.952$ ). The results of internal friction angles were generally consistent with the results presented by Miccio et al. (2011) for woody biomass and by Stasiak et al. (2015) for sawdust and wood shavings.

On the other hand, the external friction angle  $\delta$  was negatively correlated with  $x_g$  ( $r=-0.945$ , almost full correlation) and with effective angle of internal friction

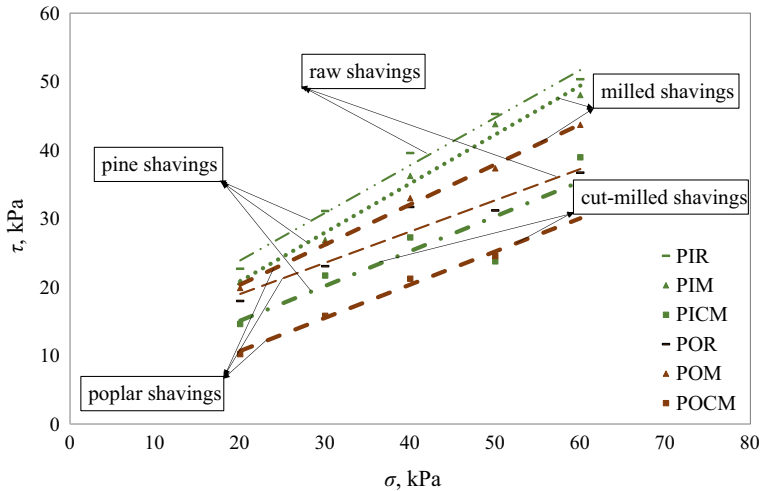


**Fig. 5** Shear stress ( $\tau$ ) related to the consolidating stress ( $\sigma$ ) for pine and poplar shavings; raw, milled and cut-milled; PIR–raw pine shavings, PIM–milled pine shavings, PICM–cut-milled pine shavings, POR–raw poplar shavings, POM–milled poplar shavings, POCM–cut-milled poplar shavings

$\varphi_e$ ,  $r = -0.435$ . The shavings with larger particles and complex shape had a smaller actual contact surface area with chrome steel surface and probably touched the peaks of roughness, while the finer shavings were able to contact on a relatively larger surface, which increased adhesion and external friction  $\delta$ . Comminuted biomass with larger particles and irregular shapes had worse flowability characteristics, because it had tendency to create bridges and get stuck with protrusions (Mattsson and Kofman 2003). The tendency to creating bridges depends on the share of long and hook-shaped particles (Stasiak et al. 2015). Raw shavings were characterised by such features, but after comminution processes the shavings were uniform and had regular shapes, without hooks and therefore, their flowability increased.

Microscopic analysis of particles is needed for a better explanation of the connection between shapes and sizes of particles with mechanical properties of wood shavings.

## Conclusion

The energy consumption during comminution of raw pine and poplar shavings was determined. PSD characteristics of raw and comminuted shavings, their mathematical models and the influence of particle size on the mechanical properties of wood shavings were determined. Estimated parameters are important in the design and operation of technological machines. The energy consumption (in  $\text{kJ}\cdot\text{kg}^{-1}$ ) of cutting-milling was lower than milling and amounted to  $182 \text{ kJ}\cdot\text{kg}^{-1}$  and  $234 \text{ kJ}\cdot\text{kg}^{-1}$ , respectively, and  $293 \text{ kJ}\cdot\text{kg}^{-1}$  and  $417 \text{ kJ}\cdot\text{kg}^{-1}$ , respectively, but because the ratio of maximum mass flow rate was a few times higher for this process, cutting-milling requires a much more powerful electric motor. Plastic poplar shavings were

more difficult to comminute than hard pine shavings. Wood species and comminution mode influenced the PSD. In the milling process, the harder pine shavings were ground into smaller particles easier than plastic poplar shavings, which were crushed. In the cutting-milling process, pine shavings split into relatively larger particles vs. plastic poplar shavings, which were easier to cut. The PSD was approximated with four mathematical models, which were ranked by goodness of fit based on  $R_{\text{adj}}^2$  evaluation, and the ranking was: RRSB (94%), normal (93%), logistic (91%) and lognormal (88%). On the basis of the best-fitted RRSB model, detailed PSD parameters were determined and all PSDs were defined as „mesokurtic”, „fine skewed” and „well-graded”. Raw shavings, with larger particle sizes than comminuted ones, were characterised by lower compressibility (21%) and flowability (55%). In comparison to the milled shavings, cut-milled shavings had a higher density (24%), but were less compressible (9%) and had lower unconfined yield strength (65%). However, they had higher flowability (150%) because of lower cohesion (63%) and angles of internal friction (18%), because after cutting-milling, the particles were more spherical than elongated particles after milling. Poplar shavings had more favourable mechanical parameters but required more energy for comminution than pine shavings. In conclusion, it can be suggested to improve a more favourable cutting-milling process than just milling of raw pine and poplar shavings by keeping them moister (about 15%), because such shavings are easier to cut. It is also reasonable to use higher mass flow rates, as a result of which a lower specific energy of comminution will be achieved.

**Supplementary Information** The online version contains supplementary material available at <https://doi.org/10.1007/s00226-023-01466-6>.

**Acknowledgements** This research is part of a doctoral dissertation supported by the Ministry of Science and Higher Education in Poland. The authors thank their colleagues from the Department of Biosystems Engineering for technical assistance in the research.

**Author contributions** Conceptualization, PT and AL; methods, PT and AL; software, PT and AL; formal analysis, PT and AL; investigation, PT, AL, JG and PO; resources, PM and AL; data curation, PT and AL; writing—original draft preparation, PT; writing—review and editing, AL and JG; visualization, PT and AL; supervision, AL All the authors have read and agreed to the published version of the manuscript.

## Declarations

**Conflict of interest** The authors declare that there are no financial or commercial conflicts of interest.

**Open Access** This article is licensed under a Creative Commons Attribution 4.0 International License, which permits use, sharing, adaptation, distribution and reproduction in any medium or format, as long as you give appropriate credit to the original author(s) and the source, provide a link to the Creative Commons licence, and indicate if changes were made. The images or other third party material in this article are included in the article's Creative Commons licence, unless indicated otherwise in a credit line to the material. If material is not included in the article's Creative Commons licence and your intended use is not permitted by statutory regulation or exceeds the permitted use, you will need to obtain permission directly from the copyright holder. To view a copy of this licence, visit <http://creativecommons.org/licenses/by/4.0/>.

## References

- ANSI/ASAE S319.4 (2008) Methods for determining and expressing fineness of feed materials by sieving. ASABE Stand ASABE, St Joseph, MI, USA, 774–778
- ANSI/ASABE S424.1 (2008) Method of determining and expressing particle size of chopped forage materials by screening. ASABE Stand ASABE, St Joseph, MI, USA, 663–665
- Aydin S, Yardimci MY, Ramyar K (2007) Mechanical properties of four timber species commonly used in Turkey. *Turkish J Eng Environ Sci* 31:19–27
- Beaunac E, Leturia M, Robisson A-C et al (2022) Comparison of two powder conditioning methods to improve UO<sub>2</sub> powder flowability for press die filling. *Powder Technol* 395:1–13. <https://doi.org/10.1016/j.powtec.2021.09.003>
- Blott SJ, Pye K (2011) Gradistat: a grain size distribution and statistics package for the analysis of unconsolidated sediments. *Earth Surf Process Landforms* 26:1237–1248. [https://doi.org/10.1016/S0167-5648\(08\)70015-7](https://doi.org/10.1016/S0167-5648(08)70015-7)
- Budhu M (2007) Soil mechanics and foundations. Wiley, Danvers
- Chevanan N, Womac AR, Bitra VSP et al (2010) Bulk density and compaction behavior of knife mill chopped switchgrass, wheat straw, and corn stover. *Bioresour Technol* 101:207–214. <https://doi.org/10.1016/j.biortech.2009.07.083>
- Eisenlauer M, Teipel U (2021) Comminution energy and particulate properties of cutting and hammer-milled beech, oak, and spruce wood. *Powder Technol* 394:685–704. <https://doi.org/10.1016/j.powtec.2021.03.072>
- Esteban LS, Carrasco JE (2006) Evaluation of different strategies for pulverization of forest biomasses. *Powder Technol* 166:139–151. <https://doi.org/10.1016/j.powtec.2006.05.018>
- Eurocode 1 (2006) Part 4: Basis of design and actions on structures. Actions in silos and tanks. European Committee for Standardization, Amsterdam
- Fasina OO (2006) Flow and physical properties of switchgrass, peanut hull, and poultry litter. *Trans Am Soc Agric Biol Eng* 49:721–728
- Ganesan V, Rosentrater KA, Muthukumarappan K (2008) Flowability and handling characteristics of bulk solids and powders—A review with implications for DDGS. *Biosyst Eng* 101:425–435. <https://doi.org/10.1016/j.biosystemseng.2008.09.008>
- Gerhards CC (1982) Effect of moisture content and temperature on the mechanical properties of wood: an analysis of immediate effects. *Wood Fiber* 14:4–36
- Gil M, Schott D, Arauzo I, Teruel E (2013) Handling behavior of two milled biomass: SRF poplar and corn stover. *Fuel Process Technol* 112:76–85. <https://doi.org/10.1016/j.fuproc.2013.02.024>
- Gopalakrishnan B, Mardikar Y, Gupta D et al (2012) Establishing baseline electrical energy consumption in wood processing sawmills for lean energy initiatives: a model based on energy analysis and diagnostics. *Energy Eng J Assoc Energy Eng* 109:40–80. <https://doi.org/10.1080/01998595.2012.10531822>
- Hehar G (2013) Physicochemical and ignition properties of dust from loblolly pine wood. Auburn University
- Hopkins WG (2000) A new view of statistics. *Sportscience* 21:1–7
- Jenike AW (1961) Gravity flow of bulk solids. In: Bulletin No. 108, Utah Engineering Experiment Station, Univ. of Utah. pp 1–4
- Jewiarz M, Wróbel M, Mudryk K, Szufa S (2020) Impact of the drying temperature and grinding technique on biomass grindability. *Energies* 13:3392. <https://doi.org/10.3390/en13133392>
- Jiang J, Wang J, Zhang X, Wolcott M (2017) Characterization of micronized wood and energy-size relationship in wood comminution. *Fuel Process Technol* 161:76–84. <https://doi.org/10.1016/j.fuproc.2017.03.015>
- Jin W, Stickel JJ, Xia Y, Klinger J (2020) A Review of computational models for the flow of milled biomass Part II: continuum-mechanics models. *ACS Sustain Chem Eng* 8:6157–6172. <https://doi.org/10.1021/acssuschemeng.0c00412>
- Jung H, Lee YJ, Yoon WB (2018) Effect of moisture content on the grinding process and powder properties in food: a review. *Processes* 6:6–10. <https://doi.org/10.3390/pr6060069>
- Kratky L, Jirout T (2020) Modelling of particle size characteristics and specific energy demand for mechanical size reduction of wheat straw by knife mill. *Biosyst Eng* 197:32–44. <https://doi.org/10.1016/j.biosystemseng.2020.06.005>



- Kuptz D, Hartmann H (2014) Throughput rate and energy consumption during wood chip production in relation to raw material, chipper type and machine settings. In: Proceedings of the 22nd European biomass conference and exhibition 483–488. <https://doi.org/10.5071/22ndEUBCE2014-2CO.1.5>
- Littlefield B, Fasina OO, Shaw J et al (2011) Physical and flow properties of pecan shells-Particle size and moisture effects. *Powder Technol* 212:173–180. <https://doi.org/10.1016/j.powtec.2011.05.011>
- Mani S, Tabil LG, Sokhansanj S (2003) An overview of compaction of biomass grinds. *Powder Handl Process* 15:160–168
- Mani S, Tabil LG, Sokhansanj S (2004) Grinding performance and physical properties of wheat and barley straws, corn stover and switchgrass. *Biomass Bioenerg* 27:339–352. <https://doi.org/10.1016/j.biombioe.2004.03.007>
- Mattsson JE, Kofman PD (2003) Influence of particle size and moisture content on tendency to bridge in biofuels made from willow shoots. *Biomass Bioenerg* 24:429–435. [https://doi.org/10.1016/S0961-9534\(02\)00178-2](https://doi.org/10.1016/S0961-9534(02)00178-2)
- Mayer-Laigle C, Blanc N, Rajaonarivony RK, Rouau X (2018) Comminution of dry lignocellulosic biomass, a review: part I. From fundamental mechanisms to milling behaviour. *Bioengineering* 5:41. <https://doi.org/10.3390/bioengineering5020041>
- Miao Z, Grift TE, Hansen AC, Ting KC (2011) Energy requirement for comminution of biomass in relation to particle physical properties. *Ind Crops Prod* 33:504–513. <https://doi.org/10.1016/j.indcrop.2010.12.016>
- Miccio F, Silvestri N, Barletta D, Poletto M (2011) Characterization of woody biomass flowability. *Chem Eng Trans* 24:643–648. <https://doi.org/10.3303/CET1124108>
- Miller G (1994) The magical number seven, plus or minus two: some limits on our capacity for processing information. *Psychol Rev* 101:343–352
- Miu PI, Womac AR, Igathinathane C, Shahab S (2006) Analysis of Biomass Comminution and Separation Processes in Rotary Equipment - A Review. ASABE paper no. 066169. ASABE, St. Joseph, Michigan
- Moiceanu G, Paraschiv G, Voicu G et al (2019) Energy consumption at size reduction of lignocellulose biomass for bioenergy. *Sustain* 11:1–12. <https://doi.org/10.3390/su11092477>
- Mugabi R, Byaruhanga YB, Eskridge KM, Weller CL (2019) Performance evaluation of a hammer mill during grinding of maize grains. *Agric Eng Int CIGR J* 21:170–179
- Naimi LJ, Collard F, Bi X et al (2016) Development of size reduction equations for calculating power input for grinding pine wood chips using hammer mill. *Biomass Convers Biorefinery* 6:397–405. <https://doi.org/10.1007/s13399-015-0195-1>
- Oyedede O, Gitman P, Qu J, Webb E (2020) Understanding the impact of lignocellulosic biomass variability on the size reduction process: a review. *ACS Sustain Chem Eng* 8:2327–2343. <https://doi.org/10.1021/acssuschemeng.9b06698>
- PN-EN 50160 (2014) Voltage characteristics in public distribution systems. Standard 1–38
- Paulrud S, Mattsson JE, Nilsson C (2002) Particle and handling characteristics of wood fuel powder: effects of different mills. *Fuel Process Technol* 76:23–39. [https://doi.org/10.1016/S0378-3820\(02\)00008-5](https://doi.org/10.1016/S0378-3820(02)00008-5)
- Piątek M, Lisowski A, Kasprzycka A, Lisowska B (2016) The dynamics of an anaerobic digestion of crop substrates with an unfavourable carbon to nitrogen ratio. *Bioresour Technol* 216:607–612. <https://doi.org/10.1016/j.biortech.2016.05.122>
- Pradhan P, Mahajani SM, Arora A (2018) Production and utilization of fuel pellets from biomass: a review. *Fuel Process Technol* 181:215–232. <https://doi.org/10.1016/j.fuproc.2018.09.021>
- Rasteiro MG, Lemos CC, Vasquez A (2008) Nanoparticle characterization by PCS: the analysis of bimodal distributions. *Part Sci Technol* 26:413–437. <https://doi.org/10.1080/02726350802367399>
- Rezaei H, Lim CJ, Lau A, Sokhansanj S (2016) Size, shape and flow characterization of ground wood chip and ground wood pellet particles. *Powder Technol* 301:737–746. <https://doi.org/10.1016/j.powtec.2016.07.016>
- Rosin P, Rammler E (1933) The laws governing the fineness of powdered coal. *J Inst Fuel* 7:29–36 (**Discussion 109–122**)
- Salehi H, Barletta D, Poletto M (2017) A comparison between powder flow property testers. *Particology* 32:10–20. <https://doi.org/10.1016/j.partic.2016.08.003>
- Stasiak M, Molenda M, Bařda M et al (2019) Mechanical characteristics of pine biomass of different sizes and shapes. *Eur J Wood Prod* 77:593–603. <https://doi.org/10.1007/s00107-019-01415-w>



- Stasiak M, Molenda M, Bańda M et al (2020) Friction and shear properties of pine biomass and pellets. *Mater (basel)* 13:3567. <https://doi.org/10.3390/MA13163567>
- Stasiak M, Molenda M, Bańda M, Gondek E (2015) Mechanical properties of sawdust and woodchips. *Fuel* 159:900–908. <https://doi.org/10.1016/j.fuel.2015.07.044>
- Stasiak M, Molenda M, Gancarz M et al (2018) Characterization of shear behaviour in consolidated granular biomass. *Powder Technol* 327:120–127. <https://doi.org/10.1016/j.powtec.2017.12.037>
- Su D, Yu M (2019) Study of corn stover particle size distribution characteristics for knife mill and hammer mill. *IOP Conf Ser Earth Environ Sci* 358:052060. <https://doi.org/10.1088/1755-1315/358/5/052060>
- Tomasetta I, Barletta D, Poletto M (2014) Correlation of powder flow properties to interparticle interactions at ambient and high temperatures. *Particuology* 12:90–99. <https://doi.org/10.1016/j.partic.2013.02.002>
- Velázquez-Martí B, Meneses-Quelal WO, Gaibor-Chavez J, Niño-Ruiz Z (2018) Review of mathematical models for the anaerobic digestion process. *Anaerob Dig*. <https://doi.org/10.5772/intechopen.80815>
- Warguła Ł, Kukla M, Wieczorek B, Krawiec P (2022) Energy consumption of the wood size reduction processes with employment of a low-power machines with various cutting mechanisms. *Renew Energy* 181:630–639. <https://doi.org/10.1016/j.renene.2021.09.039>
- Weibull W (1951) A statistical distribution function of wide applicability. *J Appl Mech Trans* 18:293–297
- Weipeng W, Jianli L, Bingzi Z et al (2015) Critical evaluation of particle size distribution models using soil data obtained with a laser diffraction method. *PLoS ONE* 10:1–18. <https://doi.org/10.1371/journal.pone.0125048>
- Wilen C, Rautalin A (1995) Safety-technical characteristics of biomass, coal and straw. Final Rep Bioenergia Res Program No 305:123
- Xu G, Lu P, Li M et al (2018) Investigation on characterization of powder flowability using different testing methods. *Exp Therm Fluid Sci* 92:390–401. <https://doi.org/10.1016/j.expthermflsci.2017.11.008>
- Yang X, Lee J, Barker DE et al (2012) Comparison of six particle size distribution models on the goodness-of-fit to particulate matter sampled from animal buildings. *J Air Waste Manag Assoc* 62:725–735. <https://doi.org/10.1080/10962247.2012.671148>
- Yu M, Womac AV, Pordesimo LO (2003) Review of biomass size reduction technology. ASAE Pap. <https://doi.org/10.13031/2013.15454>

**Publisher's Note** Springer Nature remains neutral with regard to jurisdictional claims in published maps and institutional affiliations.